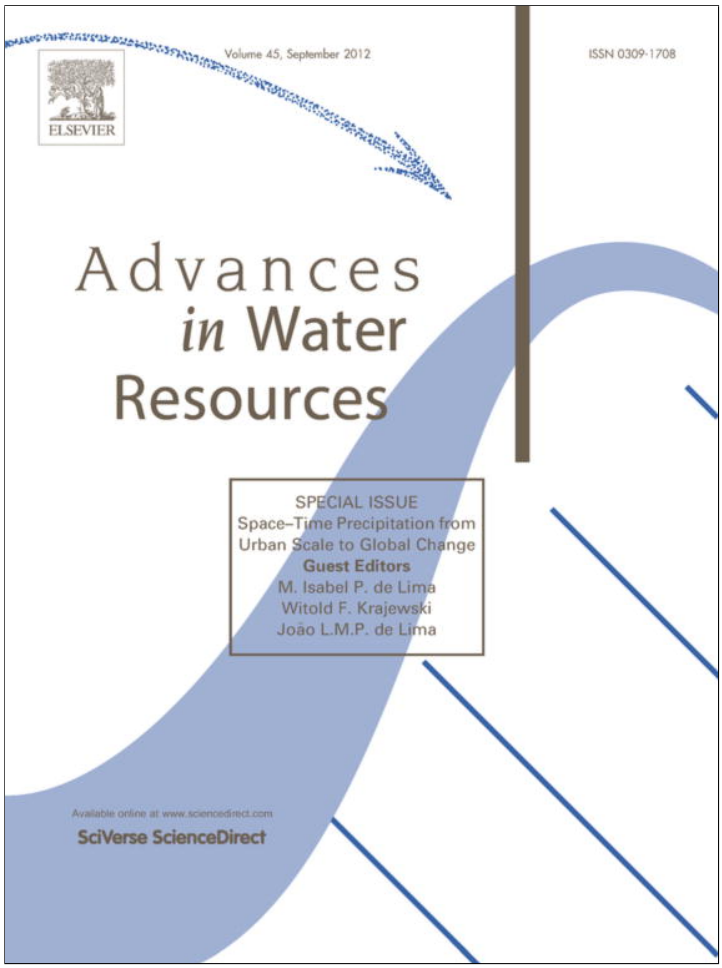

Advances in Water Resources 45 (2012) 13–25

Contents lists available at SciVerse ScienceDirect

Advances in Water Resources

journal homepage: www.elsevier.com/locate/advwatres

Influence of the zero-rainfall on the assessment of the multifractal parameters

A. Gires [a,b,*], I. Tchiguirinskaia [a,b], D. Schertzer [a,b], S. Lovejoy [c]

[a] U. Paris-Est, Ecole des Ponts ParisTech, LEESU, Marne-la-Vallée Cedex, France
[b] 6-8 Av Blaise Pascal, Cité Descartes, 77455 Marne-la-Vallée Cedex 2, France
[c] McGill U., Physics Dept., 3600 University St., H3A 2T8, Montreal, Quebec, Canada

ARTICLE INFO

Article history:
Available online 4 April 2012

Keywords:
Zero rainfall
Scale invariance
Multifractals
Truncated fields
Multifractal phase transition

ABSTRACT

Rainfall data contains numerous zero values, either real or spurious, especially at high resolution. This paper investigates how a truncation of a multifractal field affects the scaling analysis. Synthetic multifractal fields are used. The main result, which is theoretically expected and empirically observed, is that the truncated fields exhibit a multifractal phase transition for small moments. This implies an under-estimation of the multifractality index, and consequently of the extremes. This framework enables one to retrieve most of the features observed on radar data corresponding to a heavy rainfall event that occurred in September 2005 in the South of France. Finally a new technique is proposed to improve the estimation of characteristic multifractal parameters. It yields imperfect but encouraging results.

1. Introduction

Rain is extremely variable over a wide range of scales in space and time. Because of this feature the rainfall intensity is complex not only to analyze and to model, but furthermore to measure. A common way of representing such variability is to use stochastic multifractals [1–5] that basically rely on the concept of multiplicative cascades [6,7]. In the specific framework of universal multifractals (UM) that has been extensively used [1,8–16] the scaling variability of the rainfall is quantified with the help of only three scale independent parameters.

Authors have often pointed out deviations from the UM model when the rainfall field possesses numerous zeroes (i.e. numerous time steps or spatial pixels with no rain detected). Indeed, low order statistical moments are found to reflect measurement effects, such as a threshold of detection, rather than real properties of rainfall fields [11,12]. Tessier et al. [17] also mentioned that the standard technique used to estimates UM parameters might be quite sensitive to the weak events. Some authors even suggest that the threshold effect might lead to a spurious break in the scaling behavior [18,19]. In spite of the concerns that measurement effects may distort natural behavior and properties of rainfall fields, these effects remain often ignored and are rarely quantified.

In reality, these deviations from the established multifractal behavior are quite disturbing, and should therefore be addressed in depth. Although, the zero values do not influence the values of the extremes. They nevertheless influence the statistical estimates of the parameters that are used to estimate the extremes, and this can have drastic consequences. Moreover, the nature of the zeros is also usually unknown, as they can be either true zeros in a non-rainy area, or spurious ones simply related to a threshold of detection of the rainfall measurement devices. For instance, for most common tipping bucket rain gauges, three problems are well known that strongly affect the recording of light rainfall: (a) the need to wet the surface of the funnel and the two buckets after a dry period, (b) evaporation losses due to the fact that exposed water surface is usually large in relation to its volume, and (c) the discontinuous nature of the measurement [20]. Concerning radar measurements, the relation between the measured quantity (reflectivity) and desirable quantity (rain rate) is less precise for smaller rain rates (although in a logarithmic scale). The radar rainfall data is often considered to have a limit of detection of 0.2 mm/h. This detection limit was not much improved by recent dual polarization radar, since algorithms used to estimate rain rate from vertical and horizontal reflectivity do not work for rain rates below around 1.5 mm/h [21]. It is worth mentioning that the effects of zero values becomes more evident with higher space–time resolution of available data, when zero values become much more numerous compared to lower resolutions.

For multifractals defined as the small scale limit of the multiplicative cascade processes, the difference between infinitesimally small and zero values generally remain crucial with respect to many practical applications. Therefore, in this paper we investigate the threshold effect on simulated multifractal fields, mainly in terms of their influence on the scaling behavior and estimates of the UM parameters. No assumption on the nature of the threshold (i.e. associated with either a physical limit or a detection limit) is made. The universal multifractals framework is shortly presented in Section 2, and theoretical predictions concerning the influence of truncations are made in Section 3. The multifractal properties of the radar rainfall data corresponding to a heavy rainfall event

* Corresponding author.
E-mail address: auguste.gires@leesu.enpc.fr (A. Gires).

0309-1708/$ - see front matter © 2012 Elsevier Ltd. All rights reserved.
http://dx.doi.org/10.1016/j.advwatres.2012.03.026

that occurred in the south of France on September 5th, 2005 are discussed in Section 4. This shows the relevance of studying the threshold effect. The theoretical predictions are then confirmed with the help of simulated UM fields with known properties (Section 5). At last a new modified method to estimate UM parameters is suggested and tested (Section 6).

2. Multifractal cascades and methodology

We intend to discuss the fundamental difference between the multifractal fields having a full hierarchy of scales that results in some infinitesimally small values at small scales and the truncated multifractal fields with zero values below a threshold. We will denote by R_λ the field under investigation (i.e. either radar rainfall data or simulated multifractal fields) at the resolution $\lambda = L/l$, which is defined as the ratio between the outer scale L of the studied phenomenon and the observation scale l. The simulation of multifractal fields is generally achieved by building a random multiplicative cascade. For the pedagogical purposes we will use in this paper only its discrete case: while being easier to manipulate it remains sufficient to investigate the phenomena associated with the truncation of small values.

Within a discrete multiplicative cascade, each time step (in 1D) or each pixel (in 2D) is divided into λ_0 steps or λ_0^2 pixels respectively. We will use the scale ratio $\lambda_0 = 2$, which is rather usual although not mandatory. Furthermore, we will limit the explanations to the simplest 1D case. At each step of the cascade process, the value affected to the new time step is the one of the "parent" time step multiplied by a random factor. As a consequence, after n steps (the resolution of the cascade is $\lambda = \lambda_0^n$) the value of a given time step is the product of the random factors of each n previous steps of the cascade. Because multiplicative cascade processes converge under rather general conditions to Universal Multifractals (UM) [1,2,8], we use a UM cascade. In the multifractal framework, universal multifractals correspond to a broad generalization of the central limit theorem. Their two main parameters C_1 and α statistically characterize the mean intermittency and multifractality of a field. More precisely, the co-dimension C_1 characterizing the mean intermittency; it is the codimension of the singularity of the average field i.e. $C_1 = d - D_1$, where d is the embedding dimension of the field and D_1 is the fractal dimension of the support of this singularity, hence $C_1 = 0$ for a homogeneous field. The multifractality index α ($0 \leqslant \alpha \leqslant 2$) measures how fast the intermittency varies when considering singularities slightly different from the average field singularity. A multiplicative random factor of a UM cascade is indeed fully defined by C_1 and α as being $\exp\left[\left(\frac{C_1 \ln(\lambda_0)}{|\alpha-1|}\right)^{1/\alpha} L(\alpha)\right] \Big/ \lambda_0^{\frac{C_1}{\alpha-1}}$ with $L(\alpha)$ being an extremal Lévy-stable random variable of index α (i.e. $\langle \exp(qL(\alpha)) \rangle = \exp(q^\alpha)$) that can be generated with the help of the procedure given by Chambers et al. [22].

These two parameters will also be sufficient to simulate a field exhibiting a change in its scaling behavior by changing the values of α and/or C_1 after a pre-determined number of cascade steps. It is important to mention that the result of discrete multiplicative cascades is a conservative field, i.e. with the fixed parameter value $H = 0$. In the more general case of geophysical fields, the degree of non-conservation H measures the scale dependency of the average field. More details on the procedure for building multiplicative cascades, including continuous cascades and anisotropic space–time cascades, can be found in [23–25].

3. Expected multifractal behavior and phase transitions

The rainfall support corresponds to the geometric set of time and/or space with a non-zero rainfall value. Let's consider the field at resolution λ(=L/l where L is the outer scale of the phenomenon and l the observation scale), and regular time steps (in 1D) or boxes (in 2D) of size l. The "box counting" method [26–28] is based on the idea that the number of boxes needed (N_λ) to cover the rainfall support at resolution λ scales as:

$$N_\lambda \propto \lambda^{d-c_{\min}} \tag{1}$$

where $c_{\min}$ is the fractal codimension of the support and d the dimension of the embedding space.

In a more general way, it is possible to analyze the probability of exceeding not only zero but a scale-dependant threshold (λ^γ) defined with the help of the scale invariant notion of singularity (γ). If the field is multifractal, then these probabilities scale with the resolution [2] as:

$$\Pr(R_\lambda \geqslant \lambda^\gamma) \approx \lambda^{-c(\gamma)} \tag{2}$$

this defines the statistical codimension function $c(\gamma)$. This function is necessarily increasing and convex When $c(\gamma) < d$, $c(\gamma)$ can be interpreted as the fractal co-dimension of the support of the field where it exceeds λ^γ [2]. It can be shown [1] that this is equivalent to the scaling of statistical moments of arbitrary qth power:

$$\langle R_\lambda^q \rangle \approx \lambda^{K(q)} \tag{3}$$

which defines the scaling moment function $K(q)$. This function is convex. The functions $K(q)$ and $c(\gamma)$ are linked by the Legendre transform generalizing the relation found for geometric multifractals [29].

Let's consider a truncation of a multifractal field at a given resolution Λ with a threshold $T = \Lambda^{\gamma_{\min}}$ (where $\gamma_{\min}$ is the singularity associated with the threshold). All the values below T are artificially set to zero which corresponds to setting singularities $\gamma \leqslant \gamma_{\min}$ to $-\infty$. The codimension function becomes bounded by a minimum value $c_{\min} > 0$, defined by $c(\gamma_{\min}) = c_{\min}$, at least at the resolution Λ. In the framework of universal multifractals [1,2,8], the codimension function $c(\gamma)$ is given by

$$c(\gamma) = \frac{C_1}{\alpha - 1}\left(\frac{\gamma}{C_1 \alpha'} + \frac{1}{\alpha}\right)^{\alpha'} \tag{4}$$

(C_1 and α are defined in the previous section and α' satisfies $1/\alpha' + 1/\alpha = 1$) while the scaling moment function $K(q)$ corresponds to:

$$K(q) = \frac{C_1}{\alpha - 1}(q^\alpha - q) \tag{5}$$

Eq. (4) yields:

$$\gamma_{\min} = \frac{C_1 \alpha}{\alpha - 1}\left(\frac{c_{\min}}{C_1}\right)^{\frac{\alpha-1}{\alpha}} - \frac{C_1}{\alpha - 1} \tag{6}$$

Because of the Legendre transform, there is a corresponding critical order of statistical moments:

$$q_{\min} = c'(\gamma_{\min}) = \left(\frac{c_{\min}}{C_1}\right)^{\frac{1}{\alpha}} \tag{6b}$$

below which the scaling moment function $K(q)$ is linear:

$$K(q) = q\gamma_{\min} - c_{\min} \tag{7}$$

As a consequence a linear regression of $K(q)$ for small q yields estimates of $\gamma_{\min}$ and $c_{\min}$. As pointed out by a few authors [12,30,31], this behavior of truncated multifractal fields is typical of a multifractal phase transition [8,32]. More precisely, it corresponds to a second order multifractal phase transition and is analogous to that of the probable maximum order of singularity due to finite sample size [14,33–35]. Indeed with a limited number of samples, the singularities greater than γ_s (maximum observable singularity) will not be observed and the statistical moments for q greater than q_s (the

corresponding maximum observable moment) will not be reliable. More quantitatively this "sampling effect" yields to $c(\gamma) = +\infty$ for $\gamma > \gamma_s$, with $c(\gamma_s) = d + d_s$ (d_s is the sample dimension, Λ^{d_s} being equal to the number of samples). As a consequence, for $q > q_s = c'(\gamma_s)$:

$$K(q) = q\gamma_s - c(\gamma_s) \tag{7b}$$

The linearity of $K(q)$ for small and large moments has a striking consequence for the Double Trace Moment (DTM) technique that is used to estimate the parameters C_1 and α [36]. This technique is based on the fact that for multifractal fields, the scaling moment function $K(q,\eta)$ of the field $R_\lambda^{(\eta)}$, obtained by upscaling the ηth power of the maximum resolution field:

$$\left\langle (R_\lambda^{(\eta)})^q \right\rangle \approx \lambda^{K(q,\eta)} \tag{8}$$

is related in a simple manner to $K(q,1) = K(q)$:

$$K(q,\eta) = K(\eta q) - qK(\eta) \tag{8a}$$

which yields for universal multifractals (Eq. (5)):

$$K(q,\eta) = \eta^\alpha K(q) \tag{8b}$$

Therefore the multifractality index α corresponds to the slope so-called DTM curve, which is the log–log plot of $K(q,\eta)$ vs. η for fixed q. With the help of Eq. (8a), the linear expressions of $K(q)$ in Eqs. (7–7b) yield the respective values of the two plateaus of $K(q,\eta)$ for small $\eta(\eta \leqslant \eta_-(q))$ and large $\eta(\eta \geqslant \eta_+(q))$:

$$-K(q,\eta) = (q-1)c_{\min}, \quad \text{for } \eta \leq \eta_-(q) = (c_{\min}/C_1)^{1/\alpha} \tag{8c}$$

$$-K(q,\eta) = (q-1)(d+d_S), \quad \text{for } \eta \geqslant \eta_+(q) = ((d+d_S)/C_1)^{1/\alpha} \tag{8d}$$

Thus the greater the fractal co-dimension of the rainfall support $c_{\min}$, the greater the plateau of $K(q,\eta)$ corresponding to small $\eta(\eta \leqslant \eta_-(q))$, and the narrower the range of available η $(\eta_-(q) \leqslant \eta \leqslant \eta_+(q))$ over which it is legitimate to estimate α (linear portion of the DTM curve). As a consequence, these two plateaus can lead to large underestimation of α, especially given that they are associated with transitory curvatures narrowing furthermore the range of available η.

We now have a theoretical framework for directly analyzing the effects on the multifractal analysis of fields truncated at a given resolution Λ, as it is the case with rainfall. The only limitations are with respect to resolutions $\lambda < \Lambda$ due to the fact that the corresponding fields are obtained by aggregation of the initial field at resolution Λ, hence having singularities $-\infty \leqslant \gamma < \gamma_{\min}$. Numerical simulations are therefore helpful to check that these singularities are statistically irrelevant.

4. Multifractal analysis of rainfall fields

To perform simulations of multifractal fields we first need to determine an appropriate range of multifractal parameters that would allow a comparison of the simulated fields with real rainfall fields. The rainfall data analyzed in this paper corresponds to a heavy rainfall event that occurred in the south-east of France on September 5th, 2005, over an area well-known for frequent occurrences of heavy flash floods. The size of the area studied is 512×512 km^2. Sixteen hours of the event are analyzed. The data were obtained as radar mosaics from Météo-France [37]; i.e. composite maps of the reflectivities obtained – in regions of overlapping radar ranges – by interpolation. As suggested by Meteo-France, the rain rate (R) is estimated from the reflectivity (Z) with the help of the classical Marshall–Palmer relation $Z = aR^b$ [38], with $a = 200$ and $b = 1.6$ (for Z in mm^6 m^{-3} and R in mm h^{-1}). The spatial resolution of the data is 1 km in space and the temporal sampling resolution is 15 min (much larger than the temporal measurement resolution of the radar which is of the order of μs). A more precise description of the data can be found in [31]. Fig. 1 displays the total rainfall depth during the analyzed event. Spatial 2D analysis was performed on average on the whole event (i.e. each time step is seen as a realization of the same phenomenon and the average in Eqs. (3) and (8) is performed on the 64 samples).

The degree of non-conservation H is estimated with the help of a spectral analysis. Indeed for fields exhibiting a scaling behavior, the spectra possess a constant spectral slope over a large range of frequencies ($E(f) \propto f^{-\beta}$). H and β are linked by the relation $\beta = 1 + 2H - K(2)$ [17,39], which allows evaluating H.

The main results of the multifractal analysis of the radar data are shown on Fig. 2. It appears that there is not a unique scaling behavior over the whole range of studied scales, and a break occurs at around 20 km (Fig. 2(a)). Such breaks are commonly reported [12,17,40]. Therefore, in the following small scale (1–20 km) and large scale (20–500 km) regimes have been distinguished. For instance, α is greater and C_1 smaller for small scale than for large scale (Fig. 2(c)). The aim of this paper is not to analyze the cause behind this break, but only to focus on the role of the zeroes. It is important to note that the estimates of $c_{\min}$ found using either the linear behavior of $K(q)$ near zero (Fig. 2(b)), or box counting (Fig. 2(d)) are in excellent agreement.

We should start from the question of relations between the zeros of an observed data set and the main properties of UM. Let us first emphasize that with $\alpha > 1$, UM fields contain already extremely small values (especially for large resolutions λ's), which become much more numerous and smaller with $\alpha < 1$. These small values can be often considered as zero values, at least numerically. In the literature there are mainly two models to introduce extra zeros if needed within a simulated UM field M with $\alpha \neq 0$: (i) thresholding M [18,19,41], (ii) multiplying M in various contexts [42,43] by an independent field S supported by a fractal set, such as the β-model which is a UM field with $\alpha = 0$ and therefore with a unique remaining parameter $c = C_1 < 2$, the fractal co-dimension of the support. Because the dimension of the support is $2 - c < 2$, its area is zero for an infinite resolution and converges to this value for larger and larger resolutions. In the following, both models are tested with the help of numerical simulations consisting of 64 fields of size 512×512 pixels, with different sets of the UM parameters and fractal co-dimension c.

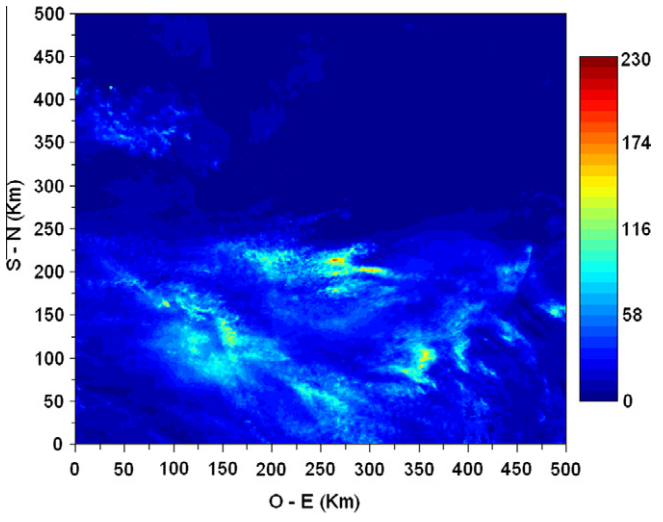

Fig. 1. Total rainfall depth (mm) during the analysed event. The coordinates (in °, Réseau géodésique français 1993 system) of the four corners are 46.3–1.3, 41.5–1.3, 46.2–8.1 et 41.4–7.5.

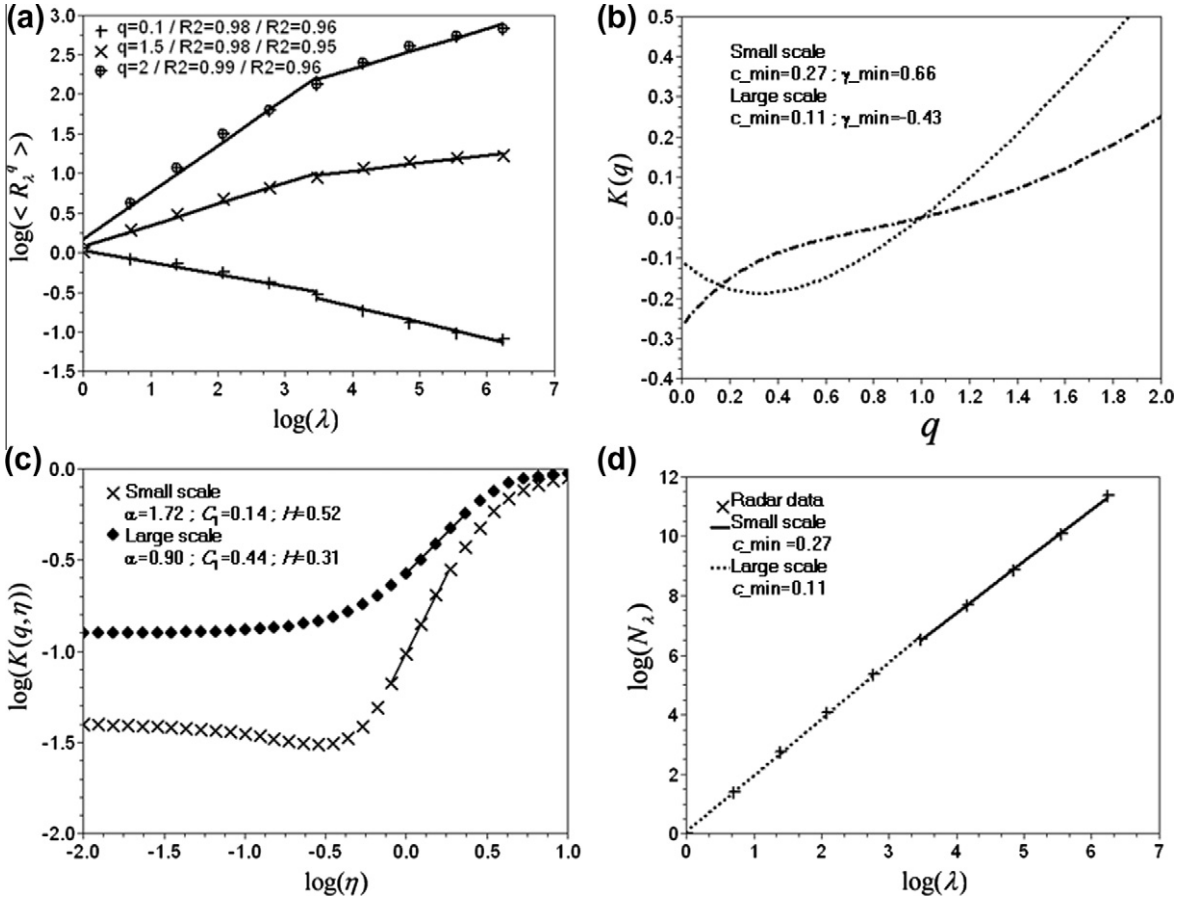

Fig. 2. Multifractal analysis of the radar data. (a) Scaling curve, i.e. Eq. (3) in a log–log plot. Large and small scales correspond respectively to the left and right part of the graph. (b) Scaling moment function $K(q)$ for $0 \leqslant q \leqslant 1$. (c) DTM curve. (d) Illustration of the box counting method (Eq. (1)).

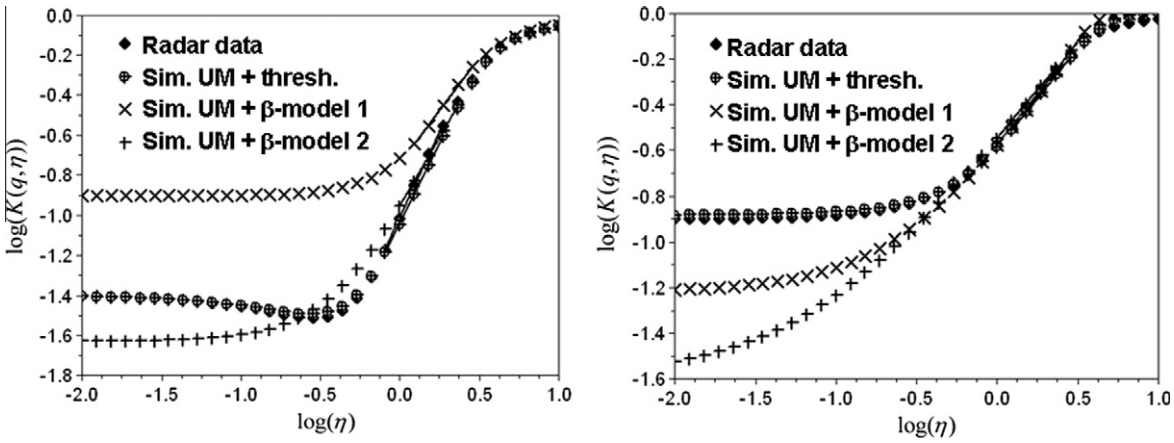

Fig. 3. DTM curves for the observed radar data, for a simulated UM field multiplied by the β-model 1 or the β-model 2 (which correspond to two β-models with different values of codimensions of the non-zero support), and a thresholded UM field. Small scales are on the left and large scales are on the right.

The first step to test the β-model hypothesis (i.e. to fit such a model) consists in retrieving the parameters of the underlying UM field [43]. In that context the rainrate field is assumed to be the product of a UM field (M) and a fully independent support (S): $R = MS$. Under the hypothesis of statistical independence of R and S, the scaling moment function of the rainfall $R = MS$ is equal to the sum of the scaling moment functions of M $K_M(q)$ (given by Eq. (5)) and S $K_S(q) = c(q-1)$, i.e. $K_R(q) = K_M(q) + K_S(q)$. Eq. (8) then yields:

$$K_R(q,\eta) = \eta^{\alpha} K(q) + c(q-1) \tag{9}$$

where c is the fractal co-dimension of the rainfall support. Once it has been estimated with the help of the box counting technique (Eq. (1)), the contribution $c(q\text{-}1)$ can be removed from the observed $K_R(q,\eta)$ before estimating the UM parameters. Applying this method on the radar data, we found $\alpha = 1.09$ and $C_1 = 0.34$ for the large scales. Concerning the small scales, it appears that the correction creates a sharp decrease on the linear part of the DTM-curve

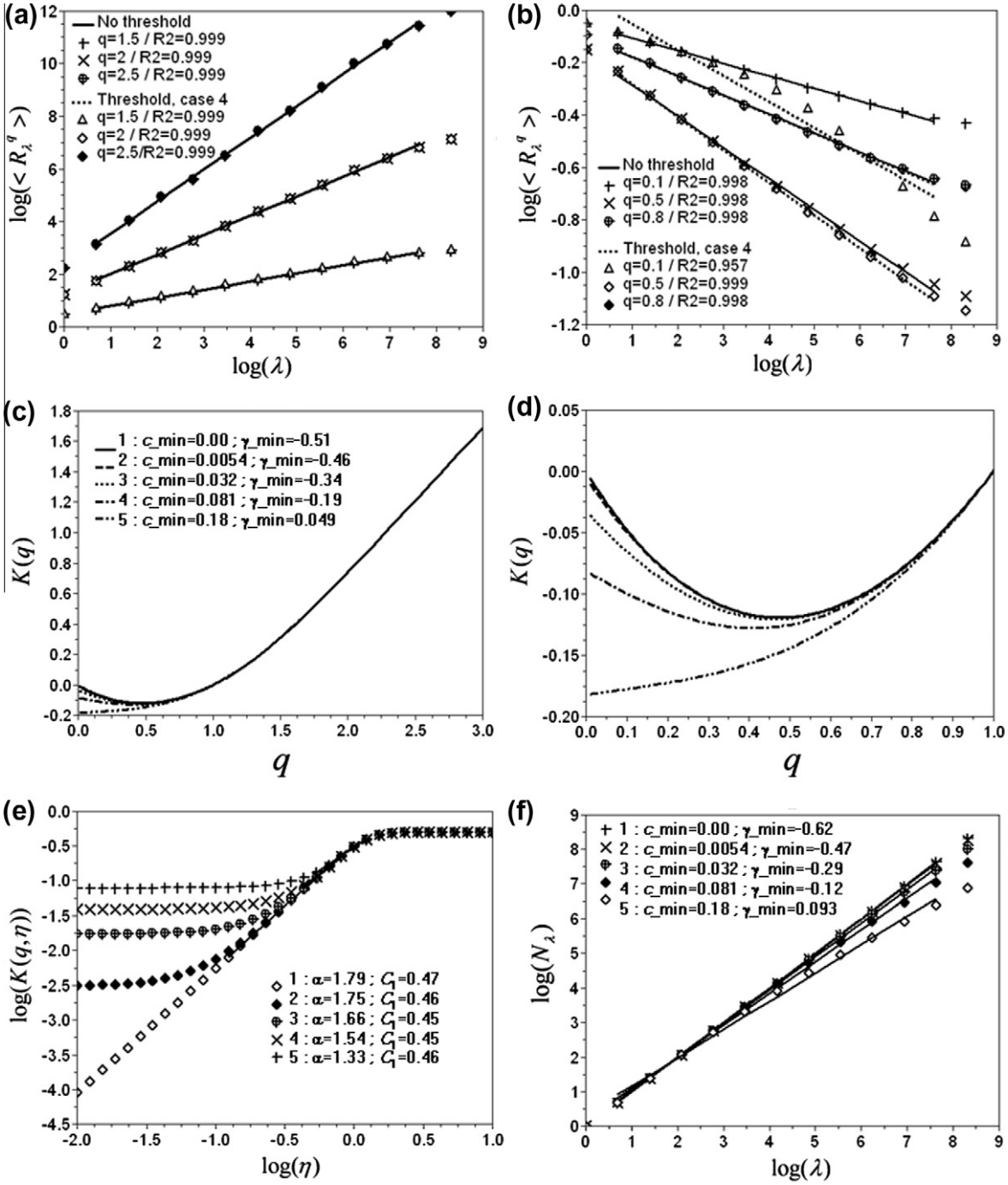

Fig. 4. Effects of the truncation (cases 1 to 5 are tested, corresponding respectively to thresholds of 0, 10^{-5}, 0.001, 0.01 and 0.1) on a simulated field with $\alpha = 1.8$ and $C_1 = 0.5$. (a) Scaling curve, i.e. Eq. (3) in a log–log plot for $q > 1$. (b) Same as in (a) for $q < 1$. (c) Scaling moment function $K(q)$ for $0 \leqslant q \leqslant 3$. (d) Scaling moment function $K(q)$ for $0 \leqslant q \leqslant 1$. (e) DTM curve. (f) Illustration of the box counting method (Eq. (1)), the determination coefficients of the curves are all above 0.995.

indicating an α value higher than its theoretical maximum of 2, and C_1 value biased low. This is the first indication that the β-model does not fit the radar data. α and C_1 are therefore fixed to respectively 2 and 0.1 for small scale. Then 64 fields of size 512×512 are simulated with these estimated parameters for the underlying UM field. With the DTM technique applied to these simulated fields the designed UM parameters are well retrieved (we find $\alpha = 1.99$ and $C_1 = 0.09$ for small scales and $\alpha = 1.09$ and $C_1 = 0.34$ for large scales).

Concerning the c parameter of the β-model, two sets of values were tested. The first set has $c = 0.27$ for small scales and $c = 0.11$ for large scales (this option is called β-model 1 in the following), which corresponds to the estimated box counting dimensions for the radar data. This leads to 69% of zeros, which is similar to the 68% of the radar data. It is important to note here the same range of scales was used for the simulated fields as for the observed ones, indeed in the very small scale limit the percentage of zero would tend toward 0. Fig. 3 displays the resulting DTM curves. They are quite different from those of the radar rainfall, and lead to $\alpha = 1.08$ and $C_1 = 0.29$ for small scales and $\alpha = 0.94$ and $C_1 = 0.42$ for large scales. The discrepancies for small scales indicate that this β-model does not fit the data. It should be mentioned that the

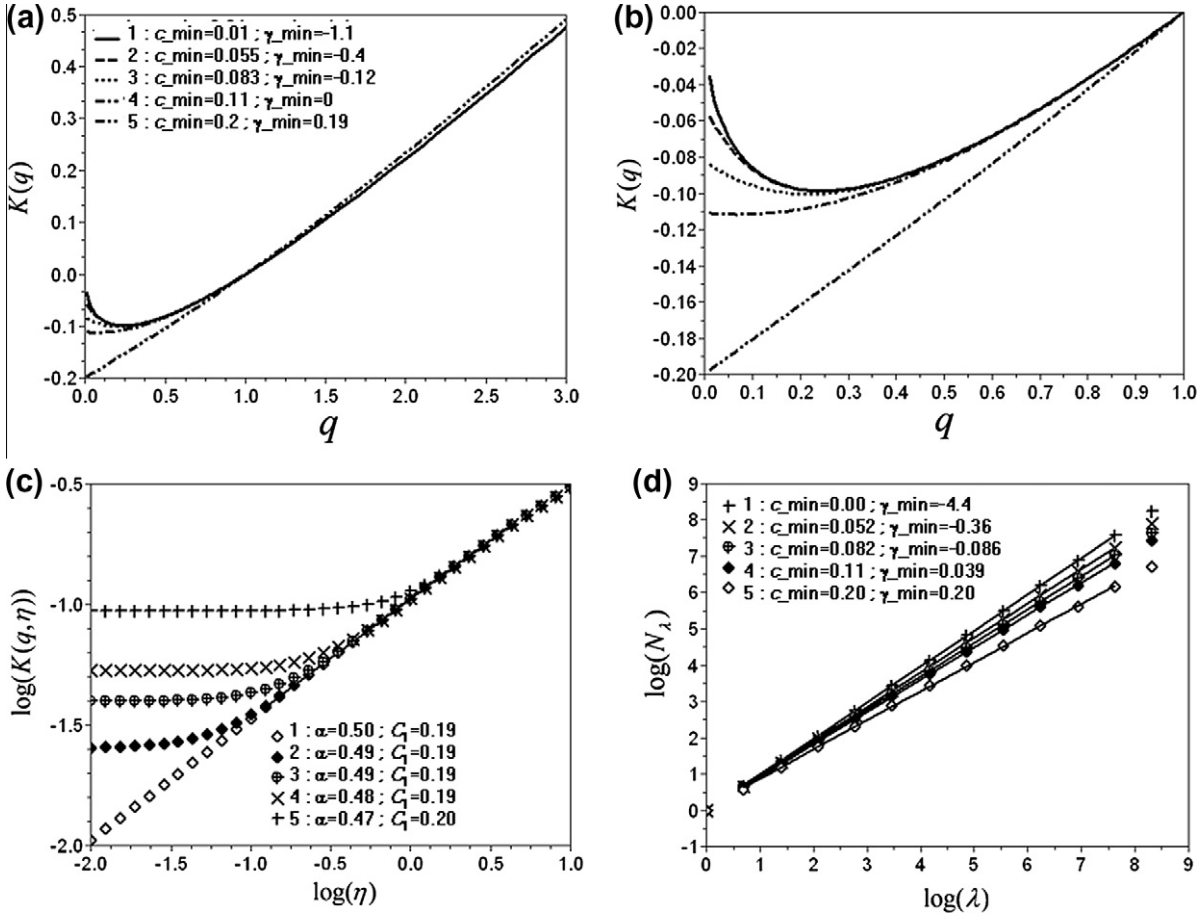

Fig. 5. Effects of the truncation (cases 1 to 5 are tested, corresponding respectively to thresholds of 10^{-80}, 10^{-10}, 10^{-5}, 10^{-3} and 10^{-1}) on a simulated field with $\alpha = 0.5$ and $C_1 = 0.2$. (a) Scaling moment function $K(q)$ for $0 \leqslant q \leqslant 3$. (b) Scaling moment function $K(q)$ for $0 \leqslant q \leqslant 1$. (c) DTM curve. (d) Illustration of the box counting method (Eq. (1)), the determination coefficients of the curves are all above 0.995.

implementation of the correction suggested by Eq. (9) enables one to retrieve the correct UM parameters. To improve the fit of the DTM curves, a second set with $c = 0.05$ for both small and large scales (this option is called β-model 2 in the following) was tested. It leads to 28% of zeros. The DTM curves (Fig. 3) are closer to the observed ones and lead to more realistic UM parameter estimates (i.e. $\alpha = 1.37$ and $C_1 = 0.17$ for small scales and $\alpha = 0.85$ and $C_1 = 0.48$ for large scales). However the co-dimension of the rainfall support and the percentage of zeros do not fit the rainfall data. Hence it appears that the two β-models tested do not fit the rainfall data set, especially for small scales where the underestimation of α and overestimation of C_1 generated by different values of c is unrealistic.

The other model for introducing zeros in a UM field, consists in thresholding it. To test it we simulated a multifractal field with the UM parameters estimated on the radar data. A threshold of 0.25 is then implemented on the normalized field (with regards to the studied rainfall field, it would corresponds to a threshold of 0.06 mm/hr which is quite close from the actual non-zero minimum value of 0.075 mm/hr) which yields 69% of zeros. The co-dimension of the support is then 0.18 for small scale and 0.20 for large scale. The DTM curves are displayed on Fig. 3. The patterns of these curves are very similar to the ones of the radar data. Indeed for both truncated simulated and observed fields the curve is constant for small and great η, and moreover there is the same slight decrease for $-1 \leqslant \eta \leqslant -0.5$. The UM parameter estimates (i.e. we find $\alpha = 1.60$ and $C_1 = 0.13$ for small scales and $\alpha = 0.87$ and $C_1 = 0.43$ for large scale) are rather similar to the one used for the simulation. This shows that the truncated simulated UM field enables to retrieve the properties of the observed radar data, and that for this specific data set the UM parameter estimates are not significantly affected by the threshold. It should be mentioned here that the potential effect of H (equal to zero the simulated field, and to 0.3 and 0.5, respectively for small and large scale for radar data) is not investigated in this paper.

As a conclusion of this section, it appears that the model consisting of a thresholding of the multifractal field almost perfectly mimics the observed behavior, whereas the hypothesis of independent support generated with the help of a β-model does not work. This fact certainly does not answer to whether the threshold corresponds to a limit of detection of the rainfall measurement device (the zero values would then be spurious) or is associated to a threshold in the physical process (the zero value would then be real). Nevertheless it shows that the zeros of the rainfall are certainly not independent from the rest of the rainfall field and hence justifies the idea that the underlying multifractal process is indeed affected by some threshold. Therefore, it seems relevant to investigate how such threshold affects the multifractal analysis.

5. Simulated multifractal fields

In this section the theoretical predictions (see Section 3) are tested with the help of simulated multifractal fields. For a given pair of UM parameters α and C_1, 1000 simulations of 4096 ($=2^{12}$) time steps are performed, and are then considered as independent

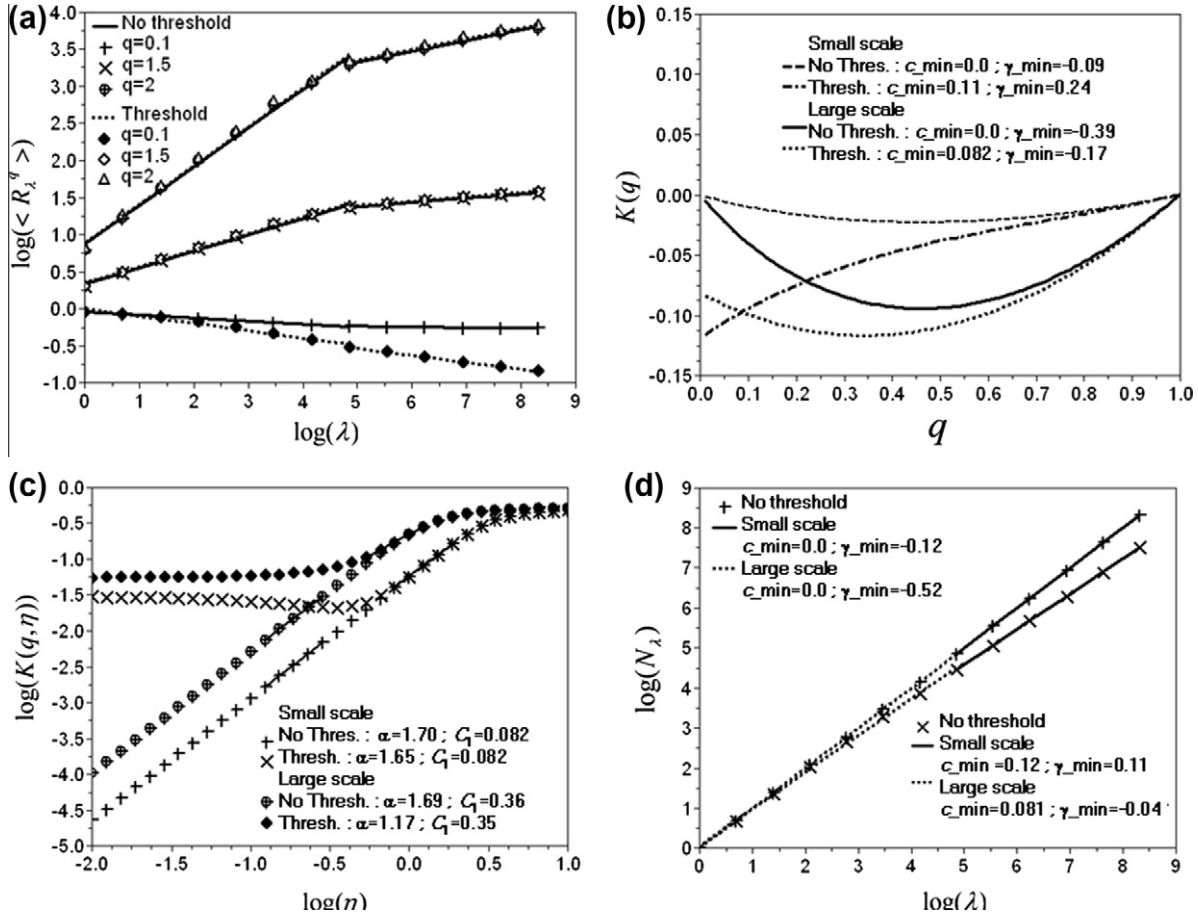

Fig. 6. Same as is Fig. 2 but for a simulated field with $\alpha = 1.7$ and $C_1 = 0.1$ for small scale and $\alpha = 1.7$ and $C_1 = 0.4$ for large scale.

samples of the same phenomenon. The above figures could be understood as 40 year records of 5 min data that was sub-divided into separate samples in order to evaluate the scaling behavior from 5 min to two weeks. The 1000 samples were ensemble averaged and normalized to unity, which allows keeping the variability among the samples. Then the truncated multifractal fields were obtained by implementing a threshold on the fields at their maximum resolution, the field was normalized again as usually done with observed rainfall data. However the mean is generally decreased by only around 1% even with the greatest thresholds that were implemented. Finally it should be mentioned that the analysis is performed on the dressed fields, i.e. the fields aggregated to a lower resolution.

5.1. Unique scaling regime with $\alpha > 1$

Based on the results of the multifractal analysis obtained from the rainfall data over the large scales, we first discuss the case of simulated multifractal fields with $\alpha = 1.8$ and $C_1 = 0.5$ over the full range of scales, i.e. displaying a unique scaling regime. Five different thresholds were used on the normalized fields: $0–10^{-5}–10^{-3}–10^{-2}–10^{-1}$, corresponding respectively to percentages of zeros equal to 0–5.4–27–51–76% in the generated field. The main curves showing the effect of the zeroes are in Fig. 4. As suggested by Marsan et al. [9] the smallest and largest scale are not included in the linear regression used to estimate $K(q)$ because they often deviate from the scaling behavior. As seen in Fig. 4(a) and (b) that display Eq. (3) in a log–log plot, the scaling behavior is excellent (determination coefficients -R^2- are greater than 0.998) on the actual field. On the truncated one, there is no change for $q > 1$ whereas the scaling is worse for small q ($R^2 = 0.95$ for $q = 0.1$). This phenomenon is expected since large order moments focus on extremes which are not affected by the thresholds, whereas small order moments focus on the small values. The curvature on the scaling curve for small q (especially visible for $q = 0.1$) means that small scales are more affected by the threshold than large scales. At resolution λ, this is a direct consequence of the truncation of the singularities, for lower resolution this is more indirect due to the upscaling process that tends to remove zero-values as the resolution decreases. This is related to the fact that the threshold is implemented at a given resolution which breaks the scaling.

For large moment orders q, the scaling moment function, $K(q)$, it is not affected by the thresholds (Fig. 4(c)), as argued above. For small orders, the expected multifractal phase transition occurs, and the linearity of $K(q)$ enables us to retrieve the intercept ($-c_{\min}$, the fractal codimension) and the slope ($\gamma_{\min}$, the minimum observable singularity). As expected $c_{\min}$ and $\gamma_{\min;}$ increase with the threshold. It is possible to evaluate these parameters with the help of another method: $c_{\min}$ is obtained by functional box counting (Eq. (1)), and then $\gamma_{\min}$ is estimated with Eq. (6) (using the parameter values α and C_1 of the simulation). The results are displayed on Fig. 4(f). Despite the poor scaling for small q, $c_{\min}$ and $\gamma_{\min}$ obtained by both methods are respectively in excellent and good agreement, which confirms the existence of the multifractal phase transition as described in the previous section. Nevertheless the observed $\gamma_{\min}$ are larger than the expected one with the formula $T = \lambda^{\gamma_{\min}}$, where T is the threshold. This is likely to be due to perturbations arising in the dressing process, and the fact that the threshold alters the quality of the scaling for small moments. It should be mentioned that the estimated spectral slope does not change when the

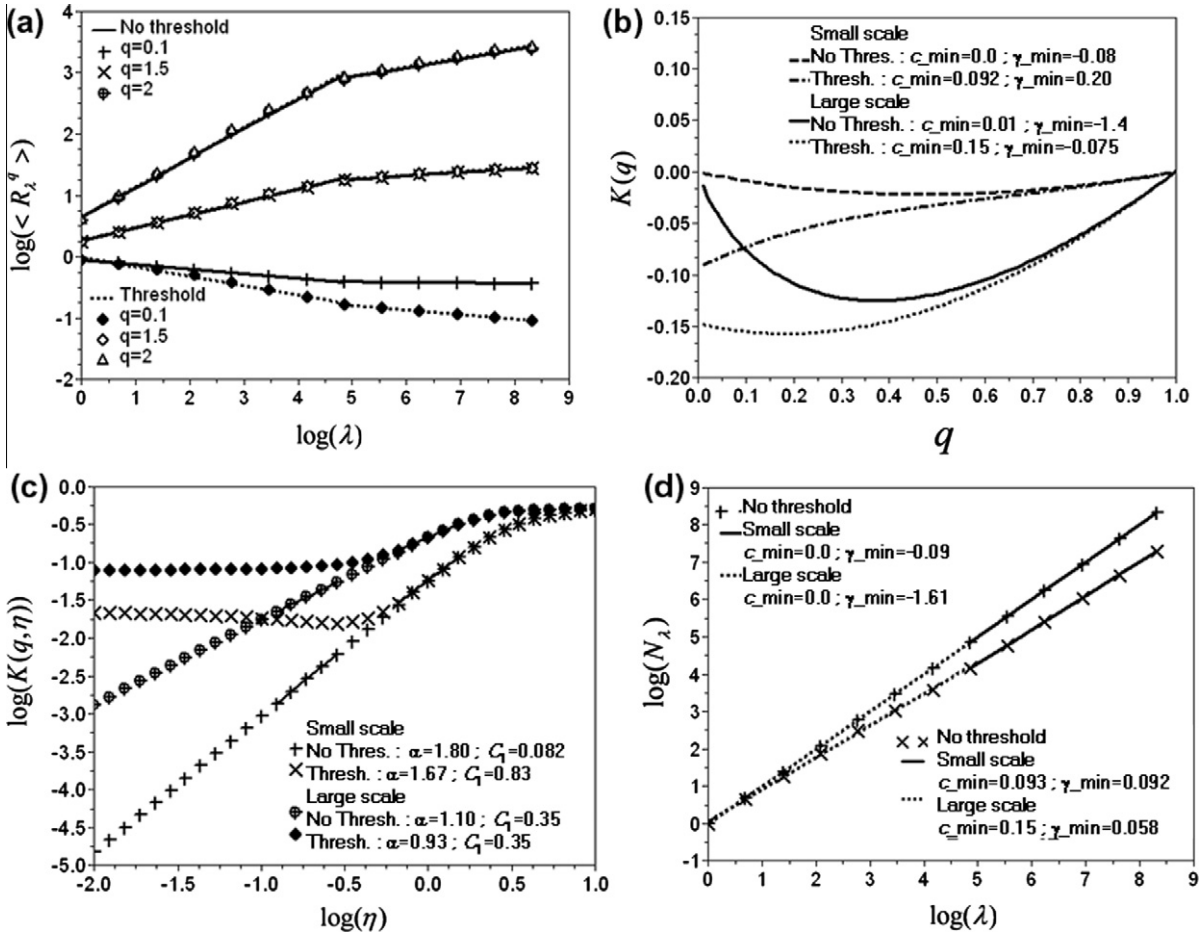

Fig. 7. Same as is Fig. 2 but for a simulated field with $\alpha = 1.8$ and $C_1 = 0.1$ for small scale and $\alpha = 1.1$ and $C_1 = 0.4$ for large scale.

field is truncated. This is not surprising since the power spectrum is equivalent to a moment of order 2, which as previously said is not affected if γ_{min} is low enough. More precisely it can theoretically be expected that statistical moments of order $q > q_{min}$ should not be too affected, with $q_{min} = c'(\gamma_{min})$, but empirically we observe an effect for higher orders.

On the DTM curve (Fig. 4(e)), the correct α and C_1 (respectively 1.79 and 0.47) are found when there is no threshold. As expected the curve levels off for large η values. The increase of the minimum value of $K(q,\eta)$ (which is in agreement with the expected value of $(q-1)c_{min}$) with the threshold, narrows the range of available η to evaluate α (the linear portion of the curve), whose estimations strongly decreases (1.33 for the greatest threshold). On the contrary, the estimates of C_1 are not significantly affected.

The same analysis performed on fields with $\alpha = 1.8$, 1.5 or 1.2 and $C_1 = 0.5$ or 0.2 yield similar results as long as γ_{min} is not too close from C_1 ($C_1 - \gamma_{min} \leqslant 0.2$ for instance). In these cases it means that too much significant portion of the field has been removed by the truncation. In these cases, even greater moments are affected.

5.2. Unique scaling regime with α<1

The same expected behavior is observed on simulations with $\alpha < 1$. Nevertheless there are few differences which are illustrated on Fig. 5. It displays the main curves showing the effect of a threshold for the simulated fields with $\alpha = 0.5$ and $C_1 = 0.2$. Five different thresholds are used $10^{-80} - 10^{-10} - 10^{-5} - 10^{-3} - 10^{-1}$, corresponding respectively to percentages of zeros equal to 19–47–59–67–79% in the generated field. It is important to note that as α and C_1 decrease, $\eta_+(q) = ((d + d_S)/C_1)^{1/\alpha}$ increases. As a consequence the DTM curve starts to level off for larger η, which widens the range of available η to evaluate α. Thus the estimates of α are less affected by the zeroes. This effect is visible on Fig. 5(c). It should also be mentioned that few difficulties arise for small thresholds when estimating γ_{min} from $K(q)$. Indeed the linearity of $K(q)$ is not very good for q around 0 (Fig. 5(b)). This is likely to be due to the fact that for $\alpha < 1$ theoretically $K'(0) = -\infty$, which is hard to deviate from. As for the case $\alpha > 1$, if γ_{min} is too close to C_1, then even large moments (i.e. $q > 1.5$) are affected. This is illustrated by the case with the largest threshold (case number 5) on Fig. 5(a), where $\gamma_{min} = 0.19$ and $C_1 = 0.2$, and $K(q)$ differs from its theoretical value for $q > 1.5$. Similar results are found for fields simulated with $\alpha = 0.5$ and $C_1 = 0.5$.

5.3. Results with a scaling break

It appears that the rainfall data exhibits a scaling break (see Section 4). This section aims at discussing some of the features of a truncated multifractal field simulated with a scaling break. The scaling break is introduced first by a change of the mean co-dimension only, and then of the multifractality parameter as well. In the first case, the same α (=1.7) was chosen on the whole range of scales, whereas $C_1 = 0.1$ for small scales and $C_1 = 0.4$ for large scales. The break is observed on the scaling curve (Fig. 6(a)) and the original UM parameters are retrieved with the DTM technique for both range of scale (Fig 6(c)). When the field is truncated, the estimates of c_{min} found with the help of the linear behavior of

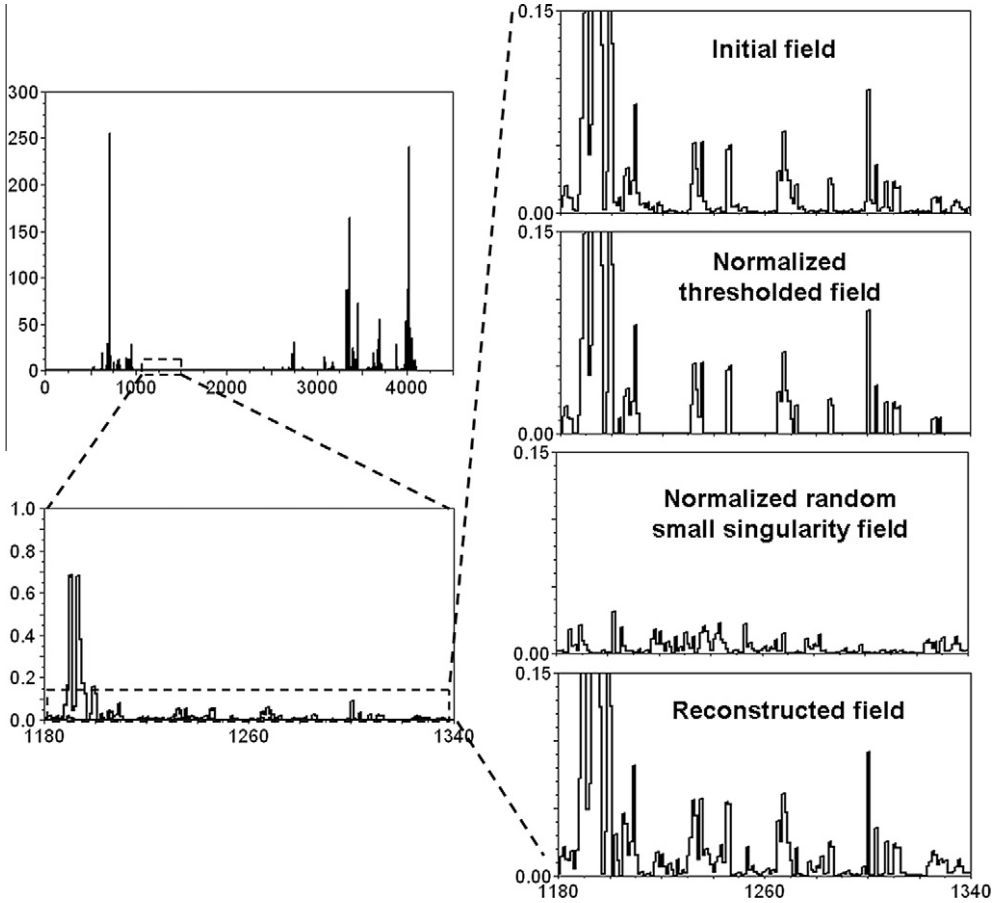

Fig. 8. Illustration of Eq. (11) for a sample with the UM parameters $\alpha = 1.8$, $C_1 = 0.5$, and a threshold of 0.01. The graphics labeled "normalized thresholded field" and "normalized random small singularity field" correspond respectively to the first and second term of the right part of Eq. (11). The "reconstructed field" is the sum of the latter two. On the left part of the figure, all the fields which are shown in separate graphs on the right part of the figure are superposed, and the vertical scale does not enable to highlight any visible differences.

$K(q)$ near zero (Fig. 6(b)), and box counting (Fig. 6(d)) are in excellent agreement, whereas the agreement (unlike in the case of the fields with no breaks) between $\gamma_{\min}$ is not very good. C_1 remains unaffected by the threshold. It is striking to note that simply by putting a threshold, significant differences are found in the estimates of α for small ($\alpha = 1.65$) and large ($\alpha = 1.17$) scale, whereas they are equal on the original field. This is due to the fact that as pointed out in the previous section, for a given α, the estimates of UM exponents of fields with greater C_1 are more affected by a threshold. It should be noted that for small scale, despite the fact that $\gamma_{\min}$ (=0.24 by estimating it with the help of the linear regression on $K(q)$ for small q) is quite superior to C_1 (=0.082) (although it should be qualified by the fact that with the box counting dimension and Eq. (6) one find $\gamma_{\min} = 0.11$), the estimates of α remains valid (equal to 1.65 instead of 1.70). This quite surprising feature is due to the fact that the determination curve of α slightly decreases for $-1 \leqslant \eta \leqslant -0.5$, which extends the range of available η to estimate α. This is likely to come from the fact that some singularities that were removed at the maximum resolution were reintroduced by the up-scaling process.

Then tests with α and C_1, both being different according to the range of scales, are performed. Simulated fields with $\alpha = 1.8$ and $C_1 = 0.1$ for small scale and $\alpha = 1.1$ and $C_1 = 0.4$ for large scale are used. The results are displayed on Fig. 7. The comments of the previous paragraph made on the field with the same α for both range of scales concerning the observation of the break (Fig. 7(a)), $c_{\min}$ and $\gamma_{\min}$ (Fig. 7(b) and (d)) remain valid. The estimates of α for both ranges of scales are affected (1.67 for small scales, and 0.93 for small scale). As previously mentioned in Section 4, the pattern of the DTM curve (Fig. 7(c)) is very similar to the one of rainfall radar (Fig. 2(c)).

6. Correction of the bias introduced by the zeroes

6.1. Correction of the field

In the previous sections, the influence of the threshold effect on multifractal analysis was underlined. This section aims at presenting a technique to thwart this effect (i.e. that enables to retrieve the actual UM exponents), that provides encouraging results while exhibiting some limitations. The actual field (without truncation) is denoted by R_λ and $R_\lambda^{(m)}$ is the measured field (with truncation). Both fields are normalized, i.e. $\langle R_\lambda \rangle = \langle R_\lambda^{(m)} \rangle = 1$. Before going on, it should be reminded that the definition of the codimension functions (Eq. (2)) leads to:

$$\langle R_\lambda \rangle \propto \int_{-\infty}^{+\infty} c'(\gamma)\lambda^{\gamma - c(\gamma)} d\gamma = \int_{-\infty}^{+\infty} f(\gamma, \alpha, C_1, \lambda) d\gamma \tag{10}$$

As pointed out in the previous section the measured field does not take into account the singularities smaller than $\gamma_{\min}$. We therefore suggest modifying the measured field at the highest resolution (Λ to give an estimate of the actual field by renormalizing it and adding a random contribution to represent the truncated singularities. Given the three parameters α, C_1 and $\gamma_{\min}$ the measured field is corrected as follows:

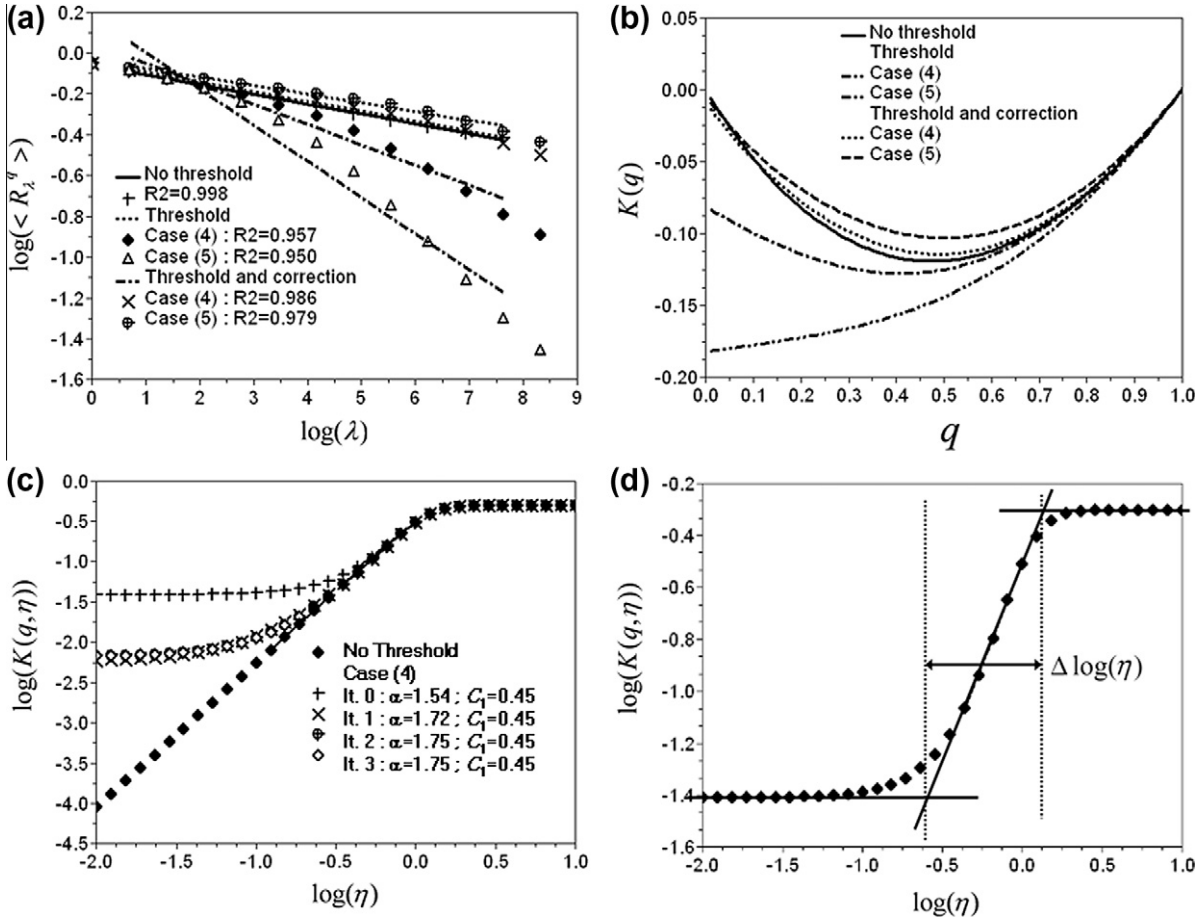

Fig. 9. Results of the multifractal analysis on the simulated field with $\alpha = 1.8$ and $C_1 = 0.5$. (a) Scaling curve, i.e. Eq. (3) in a log–log plot for $q < 1$ for the 4th and 5th threshold. (b) Scaling moment function $K(q)$ for $0 \leqslant q \leqslant 1$ for the 4th and 5th threshold. (c) DTM curve in the DTM_0 method for 4th threshold. (d) Determination curve of α on the truncated field and definition of $\Delta \log(\eta)$.

$$\hat{R}_\Lambda = R_\Lambda^{(m)} \frac{\int_{\gamma\min}^{+\infty} f(\gamma,\alpha,C_1,\Lambda)d\gamma}{\int_{-\infty}^{+\infty} f(\gamma,\alpha,C_1,\Lambda)d\gamma} + S_\Lambda^{\gamma<\gamma\min}(\alpha,C_1)\frac{\int_{-\infty}^{\gamma\min} f(\gamma,\alpha,C_1,\Lambda)d\gamma}{\int_{-\infty}^{+\infty} f(\gamma,\alpha,C_1,\Lambda)d\gamma} \tag{11}$$

where $\hat{R}_\Lambda$ is an estimate of R_λ. $S_\Lambda^{\gamma<\gamma\min}$ mimics the variability generated by the truncated singularities. To obtain this truncated field, an independent UM multifractal field with parameters α and C_1 is simulated. Then at the highest resolution, the pixels whose singularity is greater than $\gamma_{\min}$ (i.e. the value is greater to $\Lambda^{\gamma_{\min}}$) are set to zero. Finally the field is normalized to one (i.e. $\langle S_\Lambda^{\gamma<\gamma\min}\rangle = 1$). The weight factors with the integrals were chosen to ensure the normalization to unity of the estimate of the actual field $\hat{R}_\Lambda^{(a)}$. Fig. 8 illustrates Eq. (11).

In order to evaluate the UM exponents of a measured field a first guess estimate is obtained by implementing the standard DTM technique. Then a DTM analysis is performed on the field corrected according to Eq. (11) with the help of the parameters of the first parameters guess, and so on. The iterations are stopped when the difference between two successive estimates of α is below 0.01. Since the algorithm does not always converge, it is also stopped after a pre-determined number of steps (from the first implementation of the DTM technique). Details are provided below. The scaling moment function $K(q)$ is evaluated on the field corrected with the help of the final estimate of α and C_1.

6.2. Results on synthetic multifractal fields

The algorithm was tested on the truncated simulated fields. Fig. 9 displays the main results for the simulation with $\alpha = 1.8$ and $C_1 = 0.5$, which is representative of the other cases. The main differences will be pointed out below. Fig. 9(a) shows a clear improvement of the scaling behavior for small moments (increase of R^2 with the correction), which leads to a quite good correction of $K(q)$ (Fig. 9b). As expected, large order moments remain unaffected by this technique. Concerning the DTM method, the successive iterations for the fourth threshold (Table 1) are displayed on Fig. 9(c). It can be seen that the correction widens the range of available η to estimate α. The value of α obtained with the standard DTM is 1.53, and the algorithm converges towards 1.75 in three iterations, which is quite close from the value of 1.79 found on the actual field. With the fifth threshold, the algorithm does not converge. The first six estimations of α are 1.33, 1.62, 1.76, 1.85, and 1.87. This lack of convergence is also observed with large thresholds on the simulations with other UM parameters, especially when $C_1 - \gamma_{\min} \leqslant 0.2$. The divergence is faster for smaller α and greater C_1. A close analysis of the results shows that it is relevant to limit the number of iterations according to the range of available $\eta(\Delta \log(\eta))$, evaluated on the DTM curve of the truncated field (see Fig. 9(d) for an illustration). If $1.2 \leqslant \Delta \log(\eta)$ no iteration is required. If $.8 \leqslant \Delta \log(\eta) < 1.2$ then one iteration is performed. If $\Delta \log(\eta) < 0.8$ then two iterations are performed. These rules enable to perform enough iterations to obtain the correct value when the algorithm converges, and to stop it before it diverges (or converges toward a too large value of α) when necessary.

Table 1 displays the results obtained with the new algorithm (DTM_0) for all the simulations. The results are on the whole quite encouraging. The DTM_0 technique is more efficient for greater α and C_1 (for example, for the simulations with an actual α of 1.8

Table 1
Multifractal parameters for the simulated fields.

Simulated UM parameters	Threshold	c_{min}	γ_{min}	$\Delta \log(\eta)$	With threshold		Corrected	
					α	C_1	α	C_1
$\alpha = 1.8$	0	0.00	−0.51	–	1.79	0.47	1.79	0.47
$C_1 = 0.5$	10^{-5}	0.01	−0.47	1.22	1.75	0.46	1.81	0.47
	0.001	0.03	−0.34	0.87	1.66	0.45	1.76	0.46
	0.01	0.08	−0.19	0.72	1.54	0.45	1.75	0.45
	0.1	0.18	0.05	0.60	1.33	0.46	1.76	0.44
$\alpha = 1.8$	0	0.00	−0.22	–	1.80	0.19	1.80	0.19
$C_1 = 0.2$	0.01	0.01	−0.16	1.07	1.73	0.19	1.76	0.19
	0.1	0.06	−0.06	0.79	1.57	0.20	1.66	0.19
	0.3	0.11	0.04	0.69	1.42	0.22	1.65	0.19
$\alpha = 1.5$	0	0.00	−0.72	–	1.49	0.47	1.49	0.47
$C_1 = 0.5$	0.001	0.06	−0.30	0.87	1.36	0.45	1.53	0.46
	0.1	0.21	0.09	0.66	1.12	0.46	1.57	0.43
$\alpha = 1.5$	0	0.00	−0.30	–	1.51	0.19	1.51	0.19
$C_1 = 0.2$	0.1	0.07	−0.03	0.86	1.31	0.20	1.44	0.18
	0.5	0.15	0.12	0.73	1.16	0.22	1.51	0.17
$\alpha = 1.2$	0	0.00	−1.00	–	1.19	0.47	1.19	0.47
$C_1 = 0.5$	0.1	0.15	−0.09	0.84	0.99	0.44	0.99	0.44
	1	0.36	0.34	0.68	0.72	0.48	1.12	0.40
$\alpha = 1.2$	0	0.00	−0.44	–	1.20	0.19	1.20	0.19
$C_1 = 0.2$	0.01	0.05	−0.11	1.10	1.15	0.19	1.26	0.19
	0.1	0.09	0.00	0.90	1.11	0.19	1.24	0.18

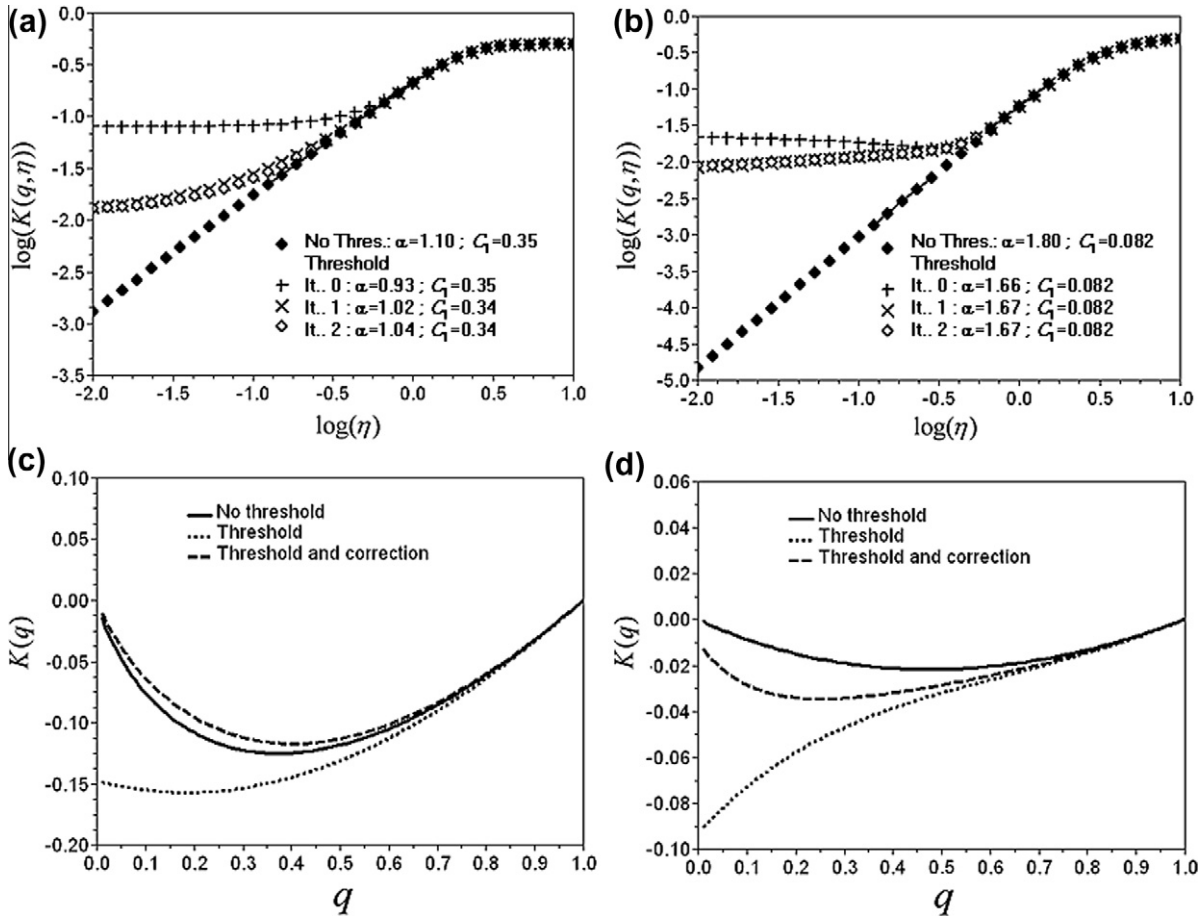

Fig. 10. Corrected multifractal analysis for the simulated field with $\alpha = 1.8$ and $C_1 = 0.1$ for small scale and $\alpha = 1.1$ and $C_1 = 0.4$ for large scale. (a) DTM curve in the DTM_0 method for large scale. (b) Same as in (a) for small scale. (c) Scaling moment function $K(q)$ for $0 \leqslant q \leqslant 1$ for large scale. (d) Same as in (c) for small scale.

the estimations of α are better for an actual C_1 of 0.5 rather than of 0.2), that is to say when the influence of the zeroes is the strongest. C_1 estimates tend to be slightly decreased by the DTM_0 technique, but not significantly. It should be reminded that when $C_1 - \gamma_{min} \leqslant 0.2$, the obtained estimates should be cautiously considered since a too significant part of the field has been removed.

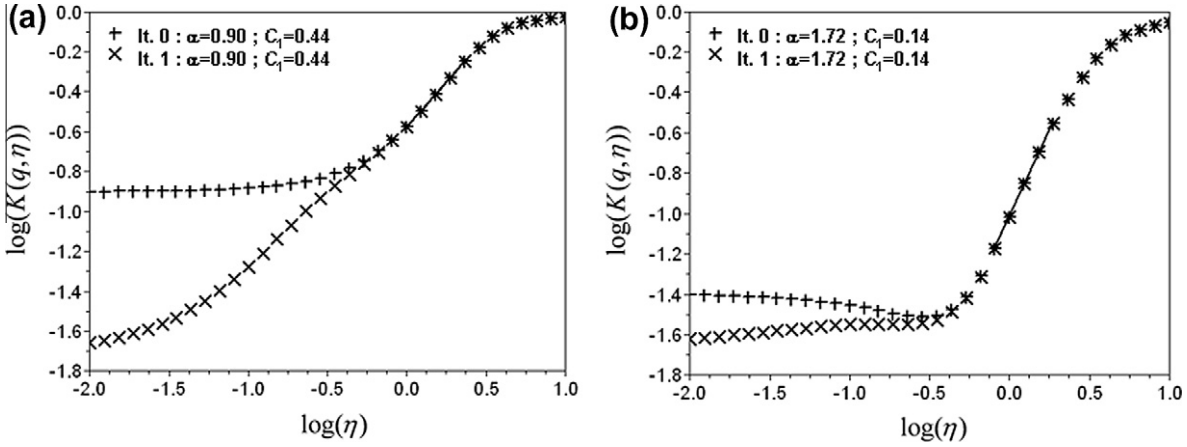

Fig. 11. Corrected multifractal analysis for the radar data. (a) DTM curve in the DTM_0 method for large scale. (b) Same as in (a) for small scale.

A limitation of the DTM_0 technique is that the stochastic field added to represent the unobserved singularities does not preserve the multiplicative structure of the original process. Moreover the robustness of the DTM_0 technique with regard to the random nature of the simulated low values should be tested. Both limitations are checked by implementing many times the DTM_0 technique on the same samples. It appears that whatever the size of the sample, the variability among the obtained estimates of UM exponents is smaller than the one existing among different samples simulated with the same UM exponents. This means that the error associated with the non-preservation of the multiplicative structure is much smaller than the one introduced by a truncation.

6.3. Results on a case with a scaling break

The DTM_0 is slightly modified when implemented on multifractal fields exhibiting a scaling break. The random field added to represent unobserved singularities ($S_A^{\gamma<\gamma\,\mathrm{min}}$, Eq. (11)) is generated with a break. The large scale $\gamma_{\min}$ is used. The number of iterations is determined according to the $\Delta\log(\eta)$ for large scales. The small scale $\gamma_{\min}$, which as pointed out in Section 5.3 is surprisingly large, was tested and yielded worse results.

The results for the field with $\alpha = 1.8$ and $C_1 = 0.1$ for small scale and $\alpha = 1.1$ and $C_1 = 0.4$ for large scale are displayed on Fig. 10. The DTM_0 technique enables to retrieve the correct value of α for large scales (1.04 is found whereas the first guess was 0.93, Fig. 10(a)), but has almost no impact on small scale estimates (Fig. 10(b)). Concerning the correction of the scaling moment function $K(q)$, the correction is quite good for large scales (Fig. 10(c)) and not very good for small scales (Fig. 10(d)).

The results of the DTM_0 technique implemented on the radar data are shown in Fig. 11. The estimates are similar to that obtained with the standard DTM (basically no change is found). This tends to confirm the results of Section 4 that the estimates of UM parameters of this specific data set are not affected by the zero values or are strongly affected by the parameter H. Further investigations on other observed rainfall fields should be performed to assess the impact of the threshold of detection on UM parameter estimates of actual measured fields.

7. Conclusion

We analyzed the effects of numerous zeros (either real or spurious) of a high-resolution rainfall field on multifractal analyses and simulations, especially with the help of the Universal Multifractals (UM). We first clarify the possible sources of the discrepancy on the proportion of zeros between observations and models, including the detection limitations. Indeed, only the monofractal β-model, i.e. the exceptional UM having a multifractality index $\alpha = 0$, has a fractal support. However, not only this model is too simplistic (only one level of rain), but we show that its multiplication with an independent UM field is not relevant, although it yields a fractal support of the same type of the β-model.

We therefore closely analysed the alternative that corresponds to thresholding a UM field. The following features are theoretically expected and observed on simulations:

- Thresholding a multifractal field is rather similar to truncating its lowest singularities, i.e. setting to $-\infty$ the singularities below a singularity $\gamma_{\min}$ corresponding to the threshold, and therefore to increasing the codimension of its support to $c_{\min} = c(\gamma_{\min})$.
- This corresponds to a second order multifractal phase transition for small moment orders q's: the scaling moment function becomes linear for the order q close to zero, and the intercept with the vertical axis ($q = 0$) and the slope of $K(q)$ are respectively equal to $c_{\min}$ and $\gamma_{\min}$.
- The scaling is deteriorated for small order moments, whereas large order moments are not affected as long as $C_1 - \gamma_{\min} \leqslant 0.2$. Otherwise it implies that a too large proportion of the field has been removed by the threshold.
- As a consequence, the range of available moments to safely estimate UM exponents becomes narrower and this easily leads to a significant under-estimation of α. The corresponding semi-analytical estimates of the extremes are therefore affected, more precisely under-estimated.
- The larger α and C_1, the larger the influence of the zeroes is.

Observed radar rainfall data, corresponding to a heavy rainfall event that occurred in the south of France in September 2005, exhibit a more complex behavior with a scaling break at about 20 km. On the whole, the multifractal phase transition is observed for both small and large scales. Most of the features of observed rainfall fields are retrieved with the help of simulated fields generated with a break (different α and C_1 for small and large scales) and then truncated.

A new multifractal analysis technique is suggested and tentatively tested to improve the estimates of UM exponents. It basically relies on renormalizing the field, adding a small random multifractal field to represent the unobserved, low singularities, and iterating the process. The technique, tested on truncated simulated fields with known exponents, enables to significantly improve the estimates as long as $C_1 - \gamma_{\min} \leqslant 0.2$. The results are much more contrasted on fields exhibiting a scaling break. Indeed small scale

estimates are almost not corrected (but are also less affected by the threshold), and large scale estimates are improved. Despite clear limitations (mainly a lack of convergence treated by limiting the number of iterations, and scaling breaks difficulties) the new techniques provides encouraging results and might be step forward in dealing with the zeroes. However further investigations are still required to improve the estimates of UM exponents in the presence of numerous zeros.

These results mean that one should be very careful when performing a multifractal analysis on high resolution rainfall fields which contain numerous zeros. Indeed a standard analysis will lead to an under-estimate of α. The influence of the multifractal phase transition for small moments should be checked to evaluate the reliability of the UM parameters estimates. A way of doing that is to implement the suggested new multifractal analysis technique.

References

[1] Schertzer D, Lovejoy S. Physical modelling and analysis of rain and clouds by anisotropic scaling and multiplicative processes. J Geophys Res 1987;92(D8): 9693–714.

[2] Schertzer D, Lovejoy S. Singularités anisotropes, divergences des moments en turbulence: invariance d'échelle généralisée et processus multiplicatifs. Ann Sci Math Que 1987;11(1):139–81.

[3] Gupta VK, Waymire E. A statistical analysis of mesoscale rainfall as a random cascade. J Appl Meteorol 1993;32:251–67.

[4] Deidda R. Rainfall downscaling in a space-time multifractal framework. Water Resour Res 2000;36:1779–94.

[5] Schertzer D, Tchiguirinskaia I, Lovejoy S, Hubert P. No monsters, no miracles: in nonlinear sciences hydrology is not an outlier! Hydrol Sci J 2010;55(6): 965–79.

[6] Yaglom AM. The influence on the fluctuation in energy dissipation on the shape of turbulent characteristics in the inertial interval. Sov Phys Dokl 1966;2:26–30.

[7] Mandelbrot B. Intermittent turbulence in self-similar cascades: divergence of high moments and dimension of the carrier. J Fluid Mech 1974;62:331–50.

[8] Schertzer D, Lovejoy S, Schmitt F, Tchiguirinskaia I, Marsan D. Multifractal cascade dynamics and turbulent intermittency. Fractals 1997;5(3):427–71.

[9] Marsan D, Schertzer D, Lovejoy S. Causal space-time multifractal processes: predictability and forecasting of rain fields. J Geophys Res 1996;101(26): 333, 326, 346.

[10] Olsson J, Niemczynowicz J. Multifractal analysis of daily spatial rainfall distributions. J Hydrol 1996;187:29–43.

[11] Harris D, Menabde M, Seed A, Austin G. Factors affecting multiscaling analysis of rainfall time series. Nonlinear Process Geophys 1997;4:137–55.

[12] de Lima MIP, Grasman J. Multifractal analysis of 15-min and daily rainfall from a semi-arid region in Portugal. J Hydrol 1999;220:1–11.

[13] Desaulnier-Soucy N, Lovejoy S, Schertzer D. The continuum limit in rain and the HYDROP experiment. J Atmos Res 2001;59–60:163–97.

[14] Lovejoy S, Schertzer D. Scaling and multifractal fields in the solid earth and topography. Nonlinear Process Geophys 2007;14:465–502.

[15] Nykanen DK. Linkages between orographic forcing and the scaling properties of convective rainfall in mountainous regions. J Hydrometeorol 2008;9: 327–47.

[16] Royer JF, Biaou A, Chauvin F, Schertzer D, Lovejoy S. Multifractal analysis of the evolution of simulated precipitation over France in a climate scenario. CR Geosci 2008;340:431–40.

[17] Tessier Y, Lovejoy S, Hubert P, Schertzer D, Pecknold S. Multifractal analysis and modeling of rainfall and river flows and scaling, causal transfer functions. J Geophy Res 1996;31D(26): 427, 426, 440.

[18] Larnder C. Observer problems in multifractals: the example of rain. M.Sc. Thesis. Montreal, Canada: McGill University; 1995.

[19] de Montera L, Barthes L, Mallet C, Gole P. The effect of rain-no rain intermittency on the estimation of the universal multifractals model parameters. J Hydrometeorol 2009;10(2):493–506.

[20] WMO, Guide to meteorological instruments and methods of observations, WMO-No. 8, 7th ed. 2008.

[21] Testud J, Le Bouar E, Obligis E, AliMehenni M. The rain profiling algorithm applied to polarimetric weather radar. J Atmos Ocean Technol 2000;17: 332–56.

[22] Chambers JM, Mallows CL, Stuck BW. A method for simulating stable random variables. J Am Stat Assoc 1976;71:p340.

[23] Pecknold S, Lovejoy S, Schertzer D, Hooge C, Malouin JF. The simulation of universal multifractals. In: Perdang JM, Lejeune A, editors. Cellular automata: prospects in astrophysical applications. World Scientific; 1993. p. 228–67.

[24] Lovejoy S, Schertzer D. On the simulation of continuous in scale universal multifractals, part I: spatially continuous processes. Comput Geosci; in press. http://dx.doi.org/10.1142/50218127411030647.

[25] Schertzer D, Lovejoy S. Multifractals, generalized scale invariance and complexity in geophysics. J Bifurcat Chaos 2011;21:3417–56.

[26] Hentschel HE, Proccacia I. The infinite number of generalized dimensions of fractals and strange attractors. Physica 1983;8D:435–44.

[27] Lovejoy S, Schertzer D, Tsonis AA. Functional box-counting and multiple elliptical dimensions in rain. Science 1987;235:1036–8.

[28] Hubert P, Carbonnel JP. Caractérisation fractale de la variabilité et de l'anisotropie des précipitations tropicales. CR Acad Sci Paris 1988;2:909–14.

[29] Parisi G, Frish U. A multifractal model of intermittency. In: Ghill M, Benzi R, Parisi G, editors. Turbulence and predictability in geophysical fluid dynamics. North Holland; 1985. p. 111–4.

[30] Hittinger F. Intercomparaison des incertitudes dans l'Analyse de Fréquence de Crues classique et l'Analyse Mutlifractale de Fréquence de Crues. ENSHMG. Grenoble : Institut National Polytechnique de Grenoble. Ing. Dipl.; 1997. p. 35.

[31] Gires A, Tchiguirinskaia I, Schertzer D, Lovejoy S. Analyses multifractales et spatio-temporelles des précipitations du modèle Méso-NH et des données radar. Hydrol Sci J 2010;56(3):380–96.

[32] Schertzer D, Lovejoy S. Hard and Soft Multifractal processes. Physica A 1992;185(1–4):187–94.

[33] Schertzer D, Lovejoy S. Nonlinear variability in geophysics: multifractal analysis and simulations. In: Pietronero, editor. Fractals: their physical origins and properties. New York: Plenum Press; 1989. p. 49–79.

[34] Hubert P, Tessier Y, Lovejoy S, Schertzer D, Schmitt F, Ladoy P, Carbonnel JP, Violette S. Multifractals and extreme rainfall events. Geophys Lett 1993;20:931–4.

[35] Douglas E, Barros A. Probable maximum precipitation estimation using multifractals: application in the eastern United States. J Hydrometeorol 2003;4:1012–24.

[36] Lavallée D, Lovejoy S, Ladoy P. Nonlinear variability and landscape topography: analysis and simulation. In: de Colas L, Lam N, editors. Fractas in geography. New-York: Prentice-Hall; 1993. p. 171–205.

[37] Parent du Châtelet J, Tabary P, Lamargue P. Evolution du réseau radar opérationnel de Météo-France pour une meilleure estimation des lames d'eau. Hydrologie Continentale 2005:49.

[38] Marshall JS, Palmer WM. The distribution of raindrops with size. J Meteorol 1948;5:165–6.

[39] Tessier Y, Lovejoy S, Schertzer D. Universal multifractals: theory and observations for rain and clouds. J Appl Meteorol 1993;32(2):223–50.

[40] Pathirana A, Herath S, Yamada T. Estimating rainfall distributions at high temporal resolutions using a multifractal model. Hydrol Earth Syst Sci 2003;7(5):668–79.

[41] Lovejoy S, Schertzer D, Allaire V. The remarkable wide range spatial scaling of TRMM precipitation. J Atmos Res 2008;90:10–32.

[42] Over TM, Gupta VK. A space-time theory of mesoscale rainfall using random cascades. J Geophys Res 1996;101(D21):26319–31.

[43] Schmitt F, Vannitsem S, Barbosa A. Modeling of rainfall time series using two-state renewal processes and multifractals. J Geophys Res 1998;103(D18):23181–93.